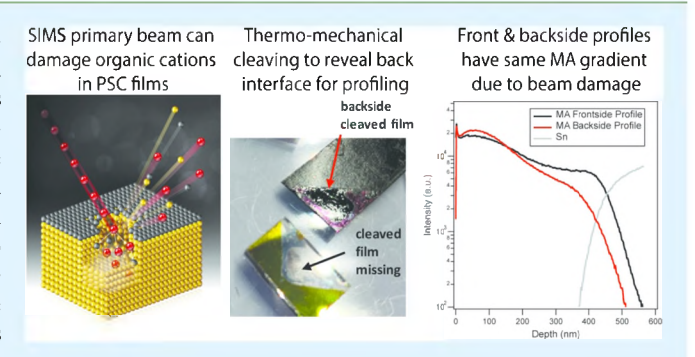
Mitigating Measurement Artifacts in TOF-SIMS Analysis of **Perovskite Solar Cells**

Steven P. Harvey,* Fei Zhang, Axel Palmstrom, Joseph M. Luther, Kai Zhu, and Joseph J. Berry

National Renewable Energy Laboratory, Golden, Colorado 80401, United States

ABSTRACT: Time-of-flight secondary ion mass spectrometry (TOF-SIMS) is one of the few techniques that can specifically distinguish between organic cations such as methylammonium and formamidinium. Distinguishing between these two species can lead to specific insight into the origins and evolution of compositional inhomogeneity and chemical gradients in halide perovskite solar cells, which appears to be a key to advancing the technology. TOF-SIMS can obtain chemical information from hybrid organicinorganic perovskite solar cells (PSCs) in up to three dimensions, while not simply splitting the organic components into their molecular constituents (C, H, and N for both



methylammonium and formamidinium), unlike other characterization methods. Here, we report on the apparently ubiquitous A-site organic cation gradient measured when doing TOF-SIMS depth-profiling of PSC films. Using thermomechanical methods to cleave perovskite samples at the buried glass/transparent conducting oxide interface enables depth profiling in a reverse direction from normal depth profiling (backside depth profiling). When comparing the backside depth profiles to the traditional front side profiled devices, an identical slight gradient in the A-site organic cation signal is observed in each case. This indicates that the apparent A-site cation gradient is a measurement artifact due to beam damage from the primary ion beam causing a continually decreasing ion yield for secondary ions of methylammonium and formamidinium. This is due to subsurface implantation and bond breaking from the 30 keV bismuth primary ion beam impact when profiling with too high of a data density. Here, we show that the beam-generated artifact associated with this damage can mostly be mitigated by altering the measurement conditions. We also report on a new method of depth profiling applied to PSC films that enables enhanced sensitivity to halide ions in positive measurement polarity, which can eliminate the need for a second measurement in negative polarity in most cases.

KEYWORDS: TOF-SIMS, PSC, HPSC, cation migration, interface, interface chemistry, passivating additive, degradation

I. INTRODUCTION

Hybrid halide perovskite solar cells (PSCs) have shown dramatic improvements in efficiency over the past decade. 1-3 Although the lack of long-term stability remains the most significant barrier to commercialization of the technology, great strides have been made in this area in only a few years.⁴ Time-of-flight secondary ion mass spectrometry (TOF-SIMS) is a characterization technique that provides detailed elemental and molecular information about the surface, thin layers, and interfaces of a sample, offering a full three-dimensional (3D) analysis. It is also one of the few analysis techniques that can differentiate the organic components of PSC materials without breaking them into their molecular constituents. Therefore, TOF-SIMS can be used to provide deep insight into the development of more efficient and reliable PSC devices, as was outlined in our previous publication related to TOF-SIMS measurements of PSC materials.8 Here, we report on the development of thermomechanical cleaving techniques for PSC materials to enable backside depth profiling in our efforts to understand the apparent organic cation gradients inherent in the TOF-SIMS profile data of PSC films. This apparently

inherent cation gradient, if real, would imply an internal gradient in the ratio of A-site to B-site cations through the thickness of the film, which would have important implications for understanding the device characteristics and performance.

SIMS is a versatile and powerful technique, but it is not without its limitations. One significant limitation of SIMS is the complex relationship between intensity and concentration, which makes quantification difficult and can affect the data in other ways, as we will discuss later in the manuscript. The SIMS intensity equation is

$$i_{A}^{S} = I^{P} Y \alpha_{A} \eta_{A} \theta_{A} X_{A} \tag{1}$$

where the measured SIMS intensity (i_A^S) depends on the primary ion intensity (I^p) , sputter yield (Y) of the ion, ionization probability $(lpha_{
m A})$ of that ion, transmission efficiency $(\eta_{\rm A})$ of the detection system, the species isotopic abundance (θ_{A}) , as well as its fractional concentration in the material

Received: May 30, 2019 Accepted: August 2, 2019 Published: August 2, 2019 $(X_{\rm A})$. Both the sputter yield and ionization probability are affected by the matrix, which means that the intensity of any secondary ion measured could be different when present in the same concentration in two different matrixes. Because the ionization probability is affected by the matrix, the signals measured can be affected by changes to the matrix. This is due to beam damage from either the primary ion beam or the sputter beam. An example of the type events that occurs from a single primary ion beam impact is shown in Figure 1.

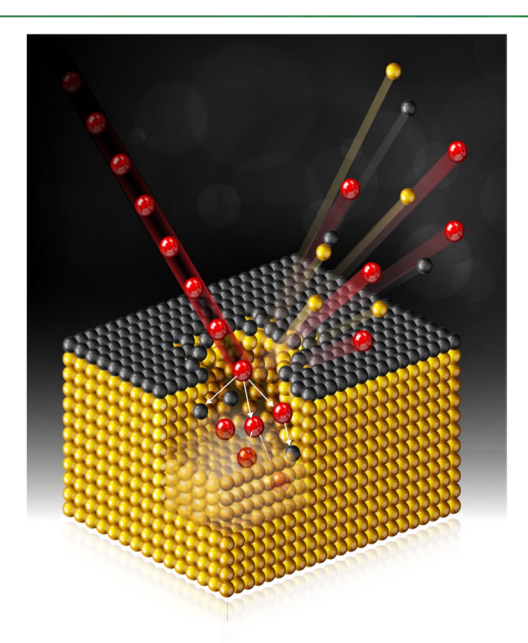


Figure 1. SIMS primary ion collision cascade results in the ejection of the sample material from the first few monolayers of the sample surface. A small amount of the ejected material is charged and we can then analyze the mass of these charged secondary ions. The primary ion beam impact also results in implantation of the primary ion into the matrix as well as the breaking of bonds and atomic mixing in the subsurface region (shown as the semitransparent area below the ion impact area). The amount of this damage depends on the energy per incident atom and the beam flux.

In dual-beam depth profiling, as is commonly employed for profiling of PSC materials, a high-energy analysis beam is used at low dosage. This induces damage, but if the ion beam flux is below the static SIMS limit of 1×10^{13} atoms/cm², we can assume that, statistically, subsequent measurements are sampling a pristine area. 9 A second low-energy etching beam is then used at higher flux to perform bulk sputtering, as the lower energy per incident ion limits the depth of beam damage induced when sputtering. When depth profiling and measuring signals for molecular organic species, as we do here for methylammonium (MA) and formamidinium (FA) in the PSC material, we are trying to liberate molecular species from the sample with the primary ion beam to form charged secondary ions of those molecular species, while trying to avoid fragmenting subsurface molecular species from the previous ion impacts, which are inherent to depth profiling. To successfully achieve this condition, three major issues must be considered, which are graphically illustrated in Figure 2: (1) the depth of damage caused by the primary ion beam impacting the sample, (2) the damage caused by the sputter source, and, when dual-beam depth profiling, which is typical for TOF-SIMS, (3) that the material removed by the sputter

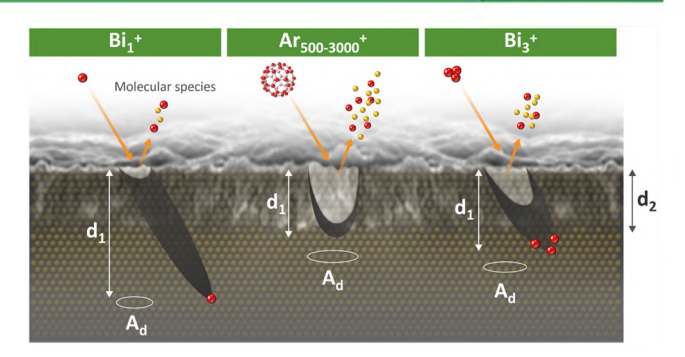


Figure 2. Illustration of some concepts related to beam damage and sputter cleanup when depth profiling molecular organic species. The relative depth of the damaged layer due to the breaking of bonds from the primary ion beam collision cascade (d_1) is shown for different primary ion beams. The 30 keV bismuth single-ion beam has the deepest damage depth, shown on the left; the argon cluster beam has the least damage depth; and the $\mathrm{Bi_3}^+$ ion beam, typically employed for perovskite depth profiling, has a damage depth between the other two ion beams. The damaged area (A_d) is inversely proportional to the damage depth d_1 , whereas the intensity of the signal for molecular organics goes in order $\mathrm{Ar}_n^+ > \mathrm{Bi_3}^+ > \mathrm{Bi_1}^+$. The material removed from one theoretical sputter cycle relative to the primary beam damage depth is shown as the sputter cycle depth d_2 . The figure created from the concepts covered in detail in Brison et al. 10

cycle should be greater than the damage depth caused by the primary beam impact. The amount of material removed in one sputter cycle is illustrated by the sputter depth " d_2 " in Figure 2, which shows the relative damage depth for different primary ion beams as " d_1 ".

Figure 2 shows the relative damage depth for different primary ion beams, the energy of the bismuth primary ion beam is typically 30 keV, whereas that for argon clusters can be varied from 2.5 to 25 keV. Because the damage depth is proportional to the energy per incident ion, the damage depth is greatest for the monatomic 30 keV bismuth beam. The damage depth can be decreased with the use of a 30 keV Bi₃⁺ cluster. This also helps generate more signal from molecular organic species as the probability of breaking subsurface bonds from the primary ion beam impact is lowered as the energy per incident ion is decreased. This can be taken to an extreme with the use of a gas cluster source, where the energy per incident ion can be as low as several eV/atom. Thus, most of the energy from the ions are then transmitted to the matrix very close to the surface, which makes the damage depth very low and the generated signals from molecular organic species very high. 10 Another important point is that the damage depth is influenced by the angle of the incident primary ion beam. This is fixed at 45° in an ION-TOF system, but if one were to have a system where the rotation of the sample was possible when profiling, then the direction of primary ion bombardment is continuously changing, which limits damage accumulation from the primary ion beam and would be more effective at depthprofiling organic species.

There are many factors which can lead to nonsuccessful depth profiling of polymeric materials (or of the organic components of the PSC film, as we do here). They are well discussed in the works by Brison and Mahoney, with more details found in the references therein. In relation to the material removed per sputter cycle (d_2 in Figure 2), if not enough material is sputtered away per cycle, the damage from bonds breaking and ionic mixing from the high-energy primary

ion beam $(d_1 \text{ in Figure 2})$ can compound with each measurement cycle. This is known as "damage accumulation", where the damage from the primary ion beam keeps compounding as each measurement cycle is sampling a volume of the sample previously damaged by the primary ion beam, and, thus, the amount of damage keeps increasing with the number of cycles. This results in more-and-more subsurface broken bonds in the MA and FA through the depth of the film during profiling. The manifestation of such damage accumulation from the primary ion beam would be a continually decreasing measured intensity for molecular species until some high-damage steady-state condition is reached. We observed this effect for FA and MA in previous work, and it is also seen in the literature. 4,8,12-16 It is often assumed that damage accumulation is avoided if the primary beam dosage is below the static SIMS limit of 1×10^{13} atoms/cm². However, this is not the only factor necessary to avoid strong measurement artifacts when TOF-SIMS depth profiling PSC materials. It is assumed that the higher the primary ion beam dosage, the more damage is imparted to the HPSC material by the primary ion beam. This would, in turn, require more material to be removed by the sputter cycle to effectively clean up the damage from the primary ion beam. This could become increasingly important when doing 3D tomography where long integration times and, thus, high dosage may be necessary to obtain highquality images for each measurement cycle in the profile.

The beam energy for the sputter sources is typically on the order of 1 keV or less, so the damage depth from the sputter beam is much lower than that for the primary beams shown in Figure 2. At higher currents (>10 nA, even at 1 keV or less), the sputter beam will certainly alter the material structure due to subsurface broken bonds, which can affect the ion yield and, thus, the intensity of the signals that are measured. Consequently, one may see differences in intensity when moving to different sputter energies or changing the sputter current. Gas cluster ion beams are ideal for investigating organic species, as the large number of atoms ensures that the energy per impact ion is low, thus the damage is more localized to the surface resulting in more efficient sputtering of molecular organic species. However, this can lead to preferential sputtering of only the organic components in mixed organic/inorganic materials like a PSC absorber. Atomic beams penetrate more deeply into the material, resulting in the breaking of bonds in the subsurface of the material. This then decreases the signal measured for a molecular species (like MA of FA) in subsequent measurement cycles.

II. EXPERIMENTAL SECTION

The hybrid perovskite solar cells used in this study were fabricated by methods discussed in detail elsewhere. The samples were analyzed by TOF-SIMS using methods discussed in detail in our previous work. Briefly, measurements were conducted in the noninterlaced mode, with a 50 \times 50 μ m² analysis area, 30 keV Bi₃⁺ primary ion beam (0.75 pA pulsed current), and a 150 × 150 μ m² sputter raster, 1 keV oxygen or cesium was used in most cases (5-8 nA current). The perovskite absorber used in this study had a composition of $(CsPbI_3)_{0.05}(FAPbI_3)_{0.85}(MAPbBr_3)_{0.15}$, where FA is formamidinium and MA is methylammonium. Alumina were deposited by atomic layer deposition (ALD) by trimethylaluminum and water at 85 °C on some films under identical conditions as our aluminum-doped zinc oxide process previously reported.¹⁷ The thermomechanical cleaving procedure used was similar to those used at NREL recently for other PV applications and have been discussed in several publications. 11 The cleaving procedure as applied to PSC materials will be discussed

in further detail here. TOF-SIMS measurements using a gas-cluster ion source for profiling were performed on the ION-TOF TOF-SIMS V instrument at the Colorado School of Mines (CSM) in this work. The primary ion beam conditions were similar to those of our previous works, but a gas-cluster ion source was used for profiling under several conditions including a 5 keV cluster energy and a 1200 argon atom cluster size (150 \times 150 $\mu \rm m^2$ area 4.5 nA), in addition to 2.5 keV cluster energy, 1000–3000 argon atom cluster size (150 \times 150 $\mu \rm m^2$ area 0.85 nA), as well as 20 keV cluster energy (500 atom cluster size–500 \times 500 $\mu \rm m^2$ area 4 nA). At both locations, the measurement conditions for profiles using oxygen and cesium for sputtering were similar to those detailed in our previous work. 8

III. RESULTS

Figure 3 shows one-dimensional depth-profile data for a 1-step-fabricated FAMACsPbI₃ film, taken from Harvey et al.⁸ In

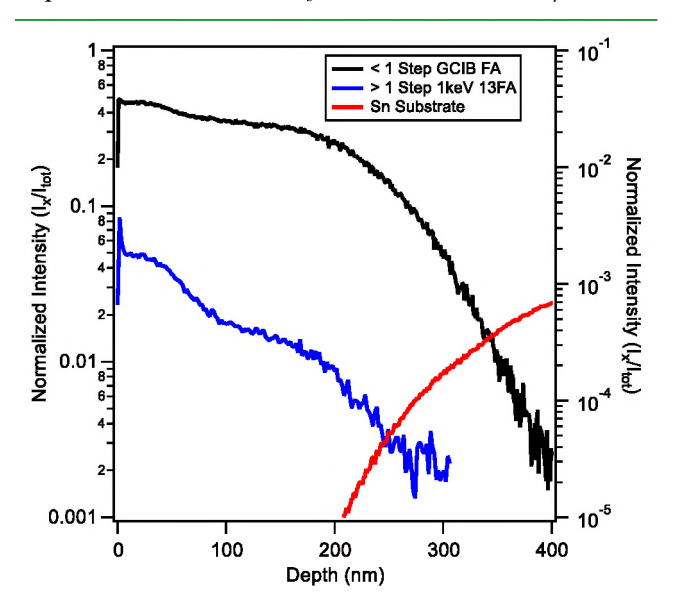


Figure 3. FA(H₂NCHNH₂) and carbon-13 FA(H₂N¹³CHNH₂) profiles normalized to total counts for 1-step prepared films. The black curves were taken with a gas-cluster ion beam (GCIB) for the sputter beam, which in theory should eliminate beam damage. The blue curve was taken with conventional low-energy oxygen as the sputter source. The GCIB FA profiles use the left-hand *y*-axis and the 13 FA profiles use the right-hand *y*-axis. An FA gradient for both films, which can be as large as an order of magnitude, is observed through the film thickness and is almost always the case. The back of the film is reached at around 250 nm, explaining the steep drop in FA signal beyond the 250 nm profile depth. Reproduced with permission from reference Harvey et al. Copyright 2018 American Chemical Society.

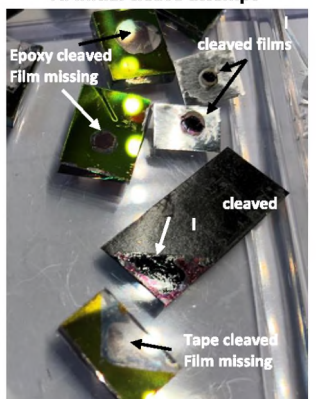
this case, data were collected both with a gas-cluster ion beam (GCIB) and with a conventional oxygen ion beam used for sputtering. The GCIB should have minimal to no beam-damage artifacts that could arise due to a change in the ionization probability for molecular species that manifest themselves as a signal with an apparent drop in intensity. However, because there was a gradient in the A-site organic cation observed through the thickness of the film in both cases, the gradient was presumed to be real. This conclusion was often met with some skepticism, as it would imply an internal gradient changing the ratio of A-site to B-site cations through the thickness of the film and is the motivation for the current study. To definitively determine if this A-site cation gradient is a measurement artifact or an inherent gradient, we employed a thermomechanical cleaving technique to separate PSC films at

the back of the device/film stack at the transparent conducting oxide (TCO)/PSC interface. By depth-profiling from both directions of the film, the A-site gradient typically observed (which decreases from the front to the back of the film) should be reversed. PSC devices are typically deposited in a superstrate stack design, where the standard PSC profile is completed with the film on glass prior to metallization. Thus, profiling is typically done from the back of the film to the front of the film, as it would be in actual operation. Here, the cleaving method to separate the film at the TCO/PSC interface exposes what is nominally the front of the PSC film in operation. However, we still refer to this as backside depth profiling due to the vernacular from the SIMS community for these types of measurements, where profiling starts from what is typically a buried interface enabled by the specialized sample preparation.

In the cleaving procedure employed previously on CdTe thin films at NREL, a thin sheet of aluminum is adhered to the CdTe with an ultra-high-vacuum compatible Torr-Seal epoxy. The sample is then placed in an argon atmosphere glovebox (<2 ppm water typical) and cured (typically overnight). Once cured, the sample is submerged in liquid nitrogen, where the sample adhered to the epoxy cleaves at the back CdTe/CdS interface due to the large difference in thermal expansion coefficient between the film stack on glass and the epoxy + metal. 18-20 When applying this to a PSC stack consisting of glass/TCO/PSC/2 nm ALD Al₂O₃/50 nm indium tin oxide (ITO), we did not have success because the epoxy reacted with the PSC absorber material, most likely due to prolonged contact before curing. By using a much thicker (~200 nm) capping TCO layer, as well as a thicker (40 nm) ALD alumina layer, the epoxy was able to cure to the metal and perovskite overnight in the glovebox without apparent degradation; it successfully cleaved when immersed in liquid nitrogen. However, a simpler approach was also successful using different types of tape adhered to the top surface and then immersed in liquid nitrogen. Several varieties of tapes were attempted including Kapton tape, scotch tape, duct tape, and electrical tape. Although cleaving worked with the epoxy + metal combo and to some extent with all tapes, as shown in Figure 4A, it worked the best with the electrical tape. When immersed in liquid nitrogen, the device cleaves reliably at the TCO/perovskite interface and the film stack is now on the tape. It should be mentioned that when cleaving the sample, it is held by the tape or metal adhered to the surface with forceps as it is lowered into the liquid nitrogen. Once the glass cleaves off (typically within a few seconds), the sample on the tape is removed from the liquid nitrogen while held under a low flow of inert gas from a spray gun for several minutes, until the sample approaches room temperature. This is done to prevent water condensation onto the sample, which could contribute to accelerated sample degradation. The tape methods were much easier from a sample preparation perspective than the epoxy + metal combo because they also dictated that the thick ITO capping layer was not needed. Thus, a new set of samples was prepared for cleaving both with and without a thin (~40 nm) ALD alumina layer on top, using only electrical tape for the cleaving. The samples without the ALD alumina consistently cleaved more uniformly, which is clearly visible in the results from the tape-only cleave attempts shown in Figure 4B.

After successful cleaving of the samples at the back TCO interface without degradation (tape and liquid nitrogen cleave), shown in Figure 4A,B, we were able to depth profile

A. Initial cleave attempt



B. Tape-only cleave results



Figure 4. (A) Photo of various cleaved samples that have been subjected to liquid nitrogen thermomechanical cleaving using the epoxy + metal or electrical tape. (B) The photo of tape-only cleave attempts; those with an ALD alumina layer on top of the PSC film are on the top of the image, marked with the text "ALD". A noncontinuous cleave is seen in these cases. The PSC-only films are at the bottom of the image, where a complete and clean cleave is noted for each film.

from the back of the device to the front. These results are shown in Figure 5, where the profile of the sample in the traditional manner (from the front surface to the back) is shown in Figure 5A. Unfortunately, the backside profile in Figure 5B shows that the organic cation gradient indeed still follows the same trend, with the increasing A-site organic content at the start of the profile (back of the device) and with decreasing intensity at the end of the profile (front of the device). These data prove that the organic cation gradient often seen in TOF-SIMS data in the literature is a measurement artifact. 4,8,12–16 Now that we know this is a measurement artifact, we performed further experiments to try to minimize the artifact by changing the measurement conditions as well as the TOF-SIMS hardware.

To investigate if the measurement artifact is due to beam damage from the sputter beam or the primary bismuth beam, we performed a series of measurements on a second ION-TOF TOF-SIMS V instrument. This instrument is similar to that at NREL, but it has some additional upgrades in the hardware such as an extended dynamic range detector and a gas-cluster ion source. With the gas-cluster ion source, a beam energy of 5 keV was used, with a cluster size of 1000 argon atoms and a sputter current of 4.5 nA. The frontside and backside depth profiles of the same sample taken under these conditions are presented in Figure 6A, where a similar gradient in the organic cations is observed as with the oxygen sputter source, as shown in Figure 5. Similar profiles were collected while further lowering the sputter beam energy to 2.5 keV (0.85 nA), still using the 1000 atom cluster size, in addition to a 2.5 keV beam energy, with a cluster size of 3000 atoms. These results were identical to those shown in Figure 5, which suggests that the bismuth primary ion beam damage is causing a reduced intensity for molecular species such as methylammonium (MA) and formamidinium (FA) as the profile is being measured. This drop in intensity due to beam damage is likely due to subsurface broken bonds altering the ionization probability for MA and FA molecular signals as the subsurface electronic structure is altered due to the beam damage.¹¹

A. Standard frontside depth profile

B. Backside cleave depth profile

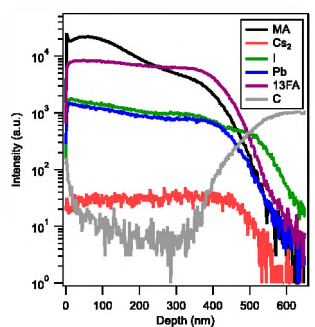
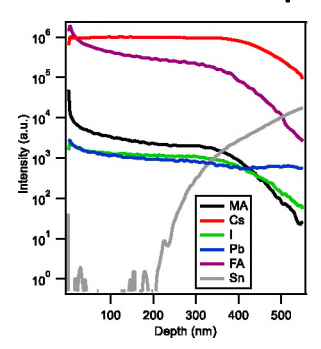


Figure 5. (A) Standard front side depth profile using our typical measurement conditions, discussed previously. A slight gradient is observed in FA, Pb, I, which is mitigated by a point-to-point normalization to total counts, not shown. The larger gradient in MA is not mitigated by normalization and shows a stronger beam-damage artifact. The Cs₂ signal increase at the back is due to a mass interference with indium, not present in the PSC portion of the profile. (B) Backside depth profile of the cleaved sample; identical gradients due to beam-damage artifacts are noted from the back of the PSC layer to the surface, which is now at the back of the profile. The sample surface is now on the electrical tape, so the carbon signal increases at the end of the profile. In both profiles, Pb refers to the 204 Pb isotope and 13 FA is the carbon-13 FA analog 13 CH(NH₂)₂, both of which are selected to avoid detector saturation. The sputter beam dose density was 1.5×10^{17} ions/cm².

A. Standard frontside depth profile B. Backside cleave depth profile



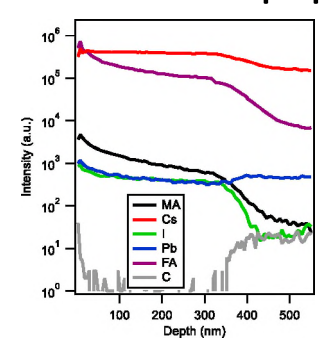


Figure 6. Profile results using a gas-cluster ion source for the sputter beam (5 keV energy, 4.5 nA, 1000 atom cluster size, 1×10^{17} ions/cm² dose density). (A) Standard frontside depth profile; similar gradients are observed to that in Figure 5. (B) Backside depth profile of the cleaved sample; again, identical gradients due to beam-damage artifacts are noted from the back of the PSC layer to the surface, which is now at the back of the profile. In both profiles, Pb refers to the 204 Pb isotope; both FA and Cs are followed in this case due to the extended dynamic range detector on the system, which avoids saturation issues in most cases.

The results shown in Figures 5 and 6 suggest that our standard measurement conditions, outlined previously,8 were leading to damage accumulation conditions for the organic cation signals when depth profiling. If this is the case, the cause would be oversampling, which happens when not enough material is being sputtered away each measurement cycle to remove damage from the primary beam between analysis cycles (see Figure 2 and the discussion covering it). The measurement conditions from the data shown in Figure 5 were then changed so that the sputter time per cycle was increased by a factor of 6× and then a factor of 12×, while keeping all other measurement parameters the same (i.e., analysis and sputter areas and dose densities). These results are shown in Figure 7, where one can clearly see that the beam-damage accumulation is mostly mitigated when the sputter time is increased between measurement cycles, and all other measurement conditions are unchanged. No change occurred when the sputter time per cycle was further increased from 30 to 60 s (not shown). This confirms that our previously published results were suffering from damage accumulation, which is also often observed in the literature as well. 4,8,12-16 With the increased sputter time between analysis cycles, the primary beam damage appears to mostly be removed between analysis cycles, as indicated by the overall increase in the MA intensity and strongly limited MA gradient at the front of the film. The beam damage is the result of primary ion beam damage accumulation, but it appears related mostly to adequate primary ion damage cleanup with sputter beam and not to primary ion beam dose density, because the measurement conditions were altered to lower the dose density from 3 × 10^{11} ions/cm² (our standard conditions) to 1×10^{10} ions/cm² (keeping the material sputtered/cycle roughly the same as the optimum 30 s condition in Figure 7), and the beam damage was identical to that shown for the 30 s sputter time/cycle in Figure 7 (not shown). In extreme cases of primary ion beam damage, one can observe an increase in the signal for the molecular fragments due to this subsurface damage, although SIMS is not a total-counting technique, typically <1% of all materials removed from the sample surface is a charged secondary ion, which can be detected. Thus, one may not always observe an increase in molecular fragments due to the beam damage, as the damage itself can alter the ion yield, which results in decreased intensities for molecular fragments as well. In the current analysis shown where beam damage is present (Figures 5-7), no significant increase in the MA or FA fragments (e.g., CH₃N⁺, CH₃⁺, signals) was noted due to the primary ion beam damage accumulation.

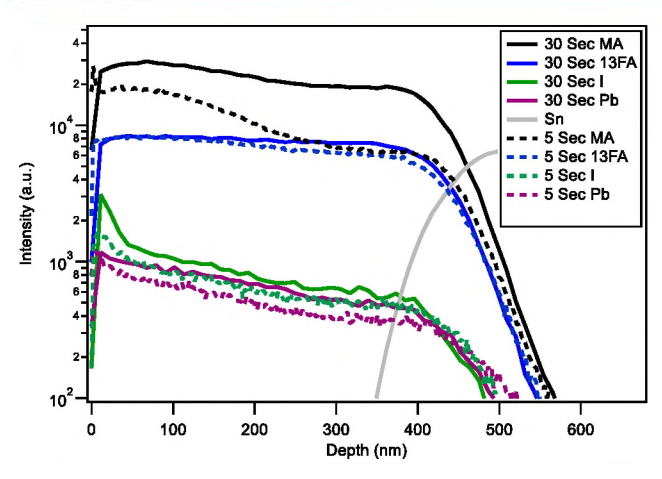


Figure 7. Depth-profile results showing reduced beam damage from the primary bismuth beam by decreasing the data density of the profile. The measurement conditions were the same as the data presented in Figure 3A, except the sputter interval between analysis cycles was increased from 5 s (same as data shown in Figure 3A, reproduced here) to 30 s. This altered the sampling rate from \sim 2 nm per datapoint to \sim 30 nm per datapoint within the PSC layer. By increasing the sputtered amount per cycle, the accumulation of beam damage from the primary bismuth beam, most prevalent in the MA signal, can be mitigated; and a more uniform FA and MA signal is observed through the film thickness. In both profiles, Pb refers to the 204 Pb isotope and 13 FA is the carbon-13 FA analog 13 CH(NH₂)₂, both of which are selected to avoid detector saturation.

Noël et al. recently reported on the effects of varying sputter beam conditions for depth-profiling PSC materials.²¹ They found, similar to our previous reports, that low-energy sputter beams (500 eV or 1 keV) are best when using monotonic sputter beams, e.g., oxygen, argon, or cesium. They also report that the best beam conditions when using a GCIS are when the energy per argon atom is rather high, 20 eV/atom or more, which ensures a proper cleanup of primary ion beam damage with each sputter cycle. This was accomplished with a small cluster size of ~500 argon atoms and a 10 or 20 keV beam energy. Measurements were then completed with a TOF-SIMS V equipped with a GCIS using these sputter beam conditions and shown in Figure 8. These results show that similar to the data shown in Figure 7, the measurement conditions originally chosen for the GCIS profiles shown in Figure 6 were also not removing enough material for each sputter cycle, resulting in a similar damage accumulation condition. The data with the increased sputter beam energy in Figure 8 now shows minimized beam damage with very uniform distribution of the organics as well as Pb and I through the film thickness.

These experiments indicate that TOF-SIMS data, although it can certainly elucidate a variety of insightful information in PSC materials and devices as we outlined in our previous publication, should be collected with the utmost care. There is the potential that beam damage can strongly affect the apparent organic cation gradients through the film thickness as well as slightly affect the apparent inorganic cation gradients. This can be partly mitigated by using a point-to-point normalization to total counts, as discussed previously. This corrects for slight changes in the ion yield, resulting in lowered measured signals, and it mitigates some of the false gradient. However, it is important for the researcher to realize that this artifact is often present in TOF-SIMS data, with varying

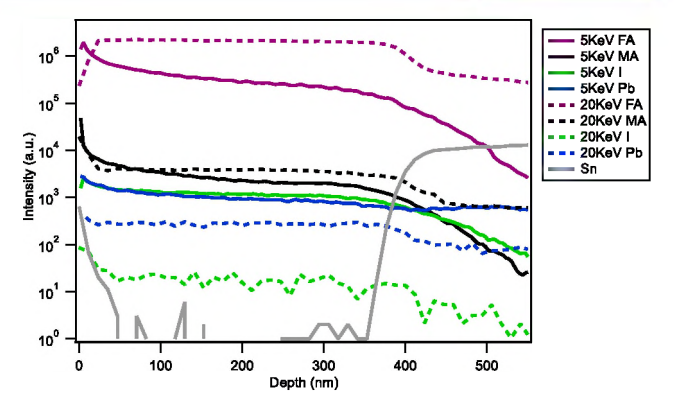


Figure 8. Depth-profile results showing reduced beam damage from the primary bismuth beam by altering the GCIS sputter energy from $\sim 5~{\rm eV/atom}$ (5 keV 1000 atom cluster data, solid lines, 1 \times 10 17 ions/cm² dose density) to $\sim 40~{\rm eV/atom}$ (20 keV to 4 nA, 500 atom cluster, dashed lines, 1 \times 10 15 ions/cm² dose density). With the 20 keV 500 atom argon cluster used as a sputter source, primary ion beam damage is mitigated, and uniform organic and inorganic cation and anion gradients are observed. Not all cation and anion species are shown for clarity. In both profiles, Pb refers to the ^{204}Pb isotope; FA, not the carbon-13 FA species, is followed in this case due to the extended dynamic range detector on the system, which can avoid saturation issues in most cases.

severity depending on measurement conditions and TOF-SIMS hardware utilized. It is also important to note that the beam damage appears to affect different organic cations to varying degrees. In Figures 5–7, one can see that the gradient observed through the thickness of the film is stronger for the MA cation than for FA. Although the mechanisms behind such relationships are unclear, presumably there would be a similarly different relationship between beam damage and ion yield in other organic cations now being employed (e.g., guanidinium thiocyanate).²² These relationships should be studied in detail if conclusions are to be made about the gradients of these species in the films.

To summarize the methods discussed here, it is suggested that a researcher conducting TOF-SIMS depth profiling of HPSC materials conduct multiple measurements under different conditions to assess what methods are working best for their absorber or film stack. We suggest using 1 keV or less oxygen or cesium for sputtering, unless a GCIS is available then that is preferred, and an energy of 40 eV/atom is recommended. Once the best possible sputter source conditions are determined for the system, one should vary the sputter interval several times when profiling to observe any changes in damage accumulation, as observed in Figures 7 and 8. If the sputter interval is too large, the data density when profiling suffers, but if the researcher has significantly altered the sputter interval (e.g., up to a factor 10×) and no changes are observed like those in Figures 7 and 8, then one can assume that the measurement conditions are optimized. Then, measurement conditions should be chosen within the bounds of sputter time/datapoint investigated that yields the desired data density within the profile.

We reported in our previous work that when looking at the halide ions in TOF-SIMS profiles, the halide signal is the strongest when doing measurements with cesium sputtering in negative polarity. Thus, one would typically have to do one profile in positive polarity and a second profile in negative polarity if detailed info about the halide ions was desired. We

A. Cesium Positive Profile

B. Organic Gradient Comparison for Difference Sputter Sources

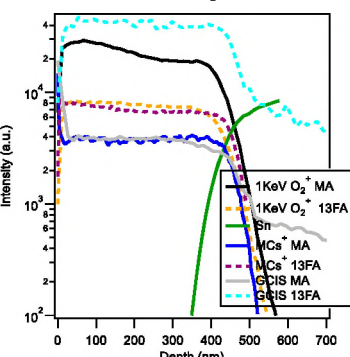


Figure 9. (A) MCs⁺ mode depth profile (1 keV Cs 6 nA 7.5×10^{16} ions/cm² dose density), where greatly enhanced halide signals are noted for the Cs₃Br₂⁺ and Cs₃I₂⁺ secondary ion clusters. (B) Comparison of the FA and MA profiles for three different measurement modes. For profiling with oxygen (also shown in Figure 6 30 s data), there is still a small amount of beam damage affecting the MA signal. With the gas-cluster ion source, there appears to be little to no beam damage (also shown in Figure 7 ~40 eV/atom data); similarly, the 1 keV Cs profiles taken in MCs⁺ mode also show very little to no beam damage in the organics.

have recently applied a standard SIMS methodology, known as MCs+ profiling, to PSC materials that greatly enhances the sensitivity of halide ions in positive measurement polarity (which is the best measurement polarity for most other PSC components). This type of analysis is typically employed to minimize effects of the matrix on the secondary ion yield when profiling alloyed or compositionally graded samples. In the analysis, a monotonic cesium beam is used as the sputter beam when profiling in positive polarity (1 keV, 6 nA in this case, 7.5 \times 10¹⁶ ions/cm² dose density). The cesium is implanted into the matrix during the sputter cycle and is, thus, sputtered away into vacuum along with the sample material from the primary ion-beam impact for an analysis cycle. Just after being sputtered from the surface, the cesium can combine with other atoms/molecules that were sputtered from the material as well to form a charged secondary ion cluster. For example, a generic metal atom "M" and the cesium, which have a very positive electronegativity, tend to enhance the generation of MCs⁺ positively charged secondary ion clusters. For example, for I or Br, one could follow CsI+ and/or CsBr+ secondary ion clusters with this type of analysis. The profile results from this measurement are shown in Figure 9; in fact, the CsI+ and CsBr⁺, as well as the Cs₂I⁺ and Cs₂Br⁺ clusters signals, were now so intense that they saturated the detector at 1×10^5 counts. We had success looking at the Cs₃Br₂⁺ and Cs₃I₂⁺ clusters with high intensity but below detector saturation. This shows an increased sensitivity to halide ions of more than 3 orders of magnitude in positive polarity (which would be even more if using an extended dynamic range analyzer, where the CsI⁺ and CsBr⁺ clusters could be followed).

Figure 9B shows the FA and MA profiles for the same film taken with optimized measurement conditions (minimized damage from the primary bismuth beam) and three different sputter beams. There is still a slight gradient noted in the MA for the oxygen sputter source, but the GCIS profile and the MCs⁺ profile show little evidence for beam damage through the thickness of the film. This measurement method induces low beam damage to the FA and MA signals, and it has the ability to sample most of the PSC material constituents with good sensitivity, including the halide ions. Therefore, this method will be heavily used in the future TOF-SIMS PSC work at NREL going forward.

IV. CONCLUSIONS

Using thermomechanical cleaving methods, we were able to profile perovskite devices from the backside. So, the profile starts at the typically buried surface of the PSC absorber and ends at what is traditionally the starting surface when profiling a PSC film. These measurements, along with standard topdown measurements on the same sample, showed that the Asite cation gradient typically measured in TOF-SIMS depth profiles is a measurement artifact due to beam damage from the bismuth primary ion beam causing decreased molecular organic signals for methylammonium and formamidinium through the profile. By altering the sputter conditions to remove more material between analysis cycles, this primary ion beam damage can be better removed, and most of the artifact can be mitigated. By switching to sputtering with a gas-cluster ion source with an energy per atom of >20 eV, it appears that there are no beam-damage artifacts in the depth profile. We also discussed a new measurement procedure applied to PSC materials, where a cesium sputter beam is used when profiling in positive polarity. This procedure yields good signal intensity for most species typically followed in a profile of a PSC material but offers significantly increased sensitivity for halide ions, as well as other very electronegative elements, e.g., bromine, sulfur, oxygen. In addition, it further minimizes beam damage compared to oxygen sputtering. This measurement mode could eliminate the need for a second depth-profile measurement in negative polarity in most cases.

AUTHOR INFORMATION

Corresponding Author

*E-mail: steve.harvey@nrel.gov.

ORCID [®]

Steven P. Harvey: 0000-0001-6120-7062 Fei Zhang: 0000-0002-3774-9520

Joseph M. Luther: 0000-0002-4054-8244

Kai Zhu: 0000-0003-0908-3909

Notes

The authors declare no competing financial interest.

ACKNOWLEDGMENTS

This work was authored by the National Renewable Energy Laboratory, operated by Alliance for Sustainable Energy, this work was supported by the U.S. Department of Energy under Contract No. DE-AC36-08GO28308 with the National Renewable Energy Laboratory. This material is based upon the work supported by the U.S. Department of Energy's Office of Energy Efficiency and Renewable Energy (EERE) under Solar Energy Technologies Office (SETO) under the project De-risking Halide Perovskite Solar Cells program, (DE-FOA-0000990) and support from the Multimode Characterization Approach for Understanding Cell-Level PV Performance and Degradation project (agreement # 34361). The authors would like to thank Dr. Craig Perkins for helpful discussions about the cleaving procedure as well as the suggestion to try various sorts of tape instead of the epoxy + metal combination, although we are still bummed that duct tape did not work the best. The authors would like to thank Michael Walker and Dr. Corinne Packard for assistance with measurements using the ION-TOF TOF-SIMS V instrument at the Colorado School of Mines. This material makes use of the TOF-SIMS system at the Colorado School of Mines, which was supported by the National Science Foundation under Grant No. 1726898. The views expressed in the article do not necessarily represent the views of the DOE or the U.S. Government. The U.S. Government retains and the publisher, by accepting the article for publication, acknowledges that the U.S. Government retains a nonexclusive, paid-up, irrevocable, worldwide license to publish or reproduce the published form of this work, or allow others to do so, for U.S. Government purposes.

■ REFERENCES

- (1) Green, M. A.; Ho-Baillie, A. Perovskite Solar Cells: The Birth of a New Era in Photovoltaics. ACS Energy Lett. 2017, 2, 822–830.
- (2) Green, M. A.; Ho-Baillie, A.; Snaith, H. J. The Emergence of Perovskite Solar Cells. *Nat. Photonics* **2014**, *8*, 506–514.
- (3) Zhang, W.; Eperon, G. E.; Snaith, H. J. Metal Halide Perovskites for Energy Applications. *Nat. Energy* **2016**, *1*, No. 16048.
- (4) Christians, J. A.; Schulz, P.; Tinkham, J. S.; Schloemer, T. H.; Harvey, S. P.; Tremolet de Villers, B. J.; Sellinger, A.; Berry, J. J.; Luther, J. M. Tailored Interfaces of Unencapsulated Perovskite Solar Cells for>1,000 Hour Operational Stability. *Nat. Energy* **2018**, *3*, 68–74.
- (5) Wang, R.; Mujahid, M.; Duan, Y.; Wang, Z.-K.; Xue, J.; Yang, Y. A Review of Perovskites Solar Cell Stability. *Adv. Funct. Mater.* **2019**, No. 1808843
- (6) Meng, L.; You, J.; Yang, Y. Addressing the Stability Issue of Perovskite Solar Cells for Commercial Applications. *Nat. Commun.* **2018**, *9*, No. 5265.
- (7) Zhang, F.; Bi, D.; Pellet, N.; Xiao, C.; Li, Z.; Berry, J. J.; Zakeeruddin, S. M.; Zhu, K.; Grätzel, M. Suppressing Defects Through the Synergistic Effect of a Lewis Base and a Lewis Acid for Highly Efficient and Stable Perovskite Solar Cells. *Energy Environ. Sci.* **2018**, *11*, 3480–3490.
- (8) Harvey, S. P.; Li, Z.; Christians, J. A.; Zhu, K.; Luther, J. M.; Berry, J. J. Probing Perovskite Inhomogeneity beyond the Surface: TOF-SIMS Analysis of Halide Perovskite Photovoltaic Devices. ACS Appl. Mater. Interfaces 2018, 10, 28541–28552.
- (9) Stevie, F. Secondary Ion Mass Spectrometry: Applications for Depth Profiling and Surface Characterization; Momentum Press, 2015.
- (10) Brison, J.; Muramoto, S.; Castner, D. G. ToF-SIMS Depth Profiling of Organic Films: A Comparison Between Single Beam and Dual-Beam Analysis. *J. Phys. Chem. C* **2010**, *114*, 5565–5573.

- (11) Mahoney, C. M. Cluster Secondary Ion Mass Spectrometry of Polymers and Related Materials. *Mass Spectrom. Rev.* **2010**, 29, 247–293.
- (12) Zhang, T.; Cheung, S.-H.; Meng, X.; Zhu, L.; Bai, Y.; Ho, C.; Xiao, S.; Xue, Q.; Kong So, S.; Yang, S. Pinning Down the Anomalous Light Soaking Effect Towards High Performance and Fast Response Perovskite Solar Cells: The Ion-Migration Induced Charge Accumulation. J. Phys. Chem. Lett. 2017, 8, 5069–5076.
- (13) Matteocci, F.; Busby, Y.; Pireaux, J.-J.; Divitini, G.; Cacovich, S.; Ducati, C.; Di Carlo, A. Interface and Composition Analysis on Perovskite Solar Cells. ACS Appl. Mater. Interfaces 2015, 7, 26176–26183.
- (14) Li, Z.; Xiao, C.; Yang, Y.; Harvey, S. P.; Kim, D. H.; Christians, J. A.; Yang, M.; Schulz, P.; Nanayakkara, S. U.; Jiang, C.-S.; Luther, J. M.; Berry, J. J.; Beard, M. C.; Al-Jassim, M. M.; Zhu, K. Extrinsic Ion Migration in Perovskite Solar Cells. *Energy Environ. Sci.* **2017**, *10*, 1234–1242
- (15) Wang, C.; Bai, Y.; Guo, Q.; Zhao, C.; Zhang, J.; Hu, S.; Hayat, T.; Alsaedi, A.; Tan, Z. Enhancing Charge Transport in an Organic Photoactive Layer via Vertical Component Engineering for Efficient Perovskite/Organic Integrated Solar Cells. *Nanoscale* **2019**, *11*, 4035–4043.
- (16) Li, J.; Dong, Q.; Li, N.; Wang, L. Direct Evidence of Ion Diffusion for the Silver-Electrode-Induced Thermal Degradation of Inverted Perovskite Solar Cells. *Adv. Energy Mater.* **2017**, *7*, No. 1602922.
- (17) Palmstrom, A. F.; Eperon, G. E.; Leijtens, T.; Prasanna, R.; Habisreutinger, S. N.; Nemeth, W.; Gaulding, E. A.; Dunfield, S. P.; Reese, M.; Nanayakkara, S.; Moot, T.; Werner, J.; Liu, J.; To, B.; Christensen, S. T.; McGehee, M. D.; van Hest, M. F. A. M.; Luther, J. M.; Berry, J. J.; Moore, D. T. Enabling Flexible All-Perovskite Tandem Solar Cells. *Joule* 2019, DOI: 10.1016/j.joule.2019.05.009.
- (18) McGott, D. L.; Kempe, M. D.; Glynn, S.; Bosco, N.; Barnes, T. M.; Haegel, N. M.; Wolden, C. A.; Reese, M. O. Thermomechanical Lift-Off and Recontacting of CdTe Solar Cells. *ACS Appl. Mater. Interfaces* **2018**, *10*, 44854–44861.
- (19) Perkins, C. L.; Beall, C.; Reese, M. O.; Barnes, T. M. Two-Dimensional Cadmium Chloride Nanosheets in Cadmium Telluride Solar Cells. *ACS Appl. Mater. Interfaces* **2017**, *9*, 20561–20565.
- (20) Perkins, C. L.; McGott, D. L.; Reese, M. O.; Metzger, W. K. SnO2-Catalyzed Oxidation in High-Efficiency CdTe Solar Cells. ACS Appl. Mater. Interfaces 2019, 11, 13003–13010.
- (21) Noël, C.; Pescetelli, S.; Agresti, A.; Franquet, A.; Spampinato, V.; Felten, A.; di Carlo, A.; Houssiau, L.; Busby, Y. Hybrid Perovskites Depth Profiling with Variable-Size Argon Clusters and Monatomic Ions Beams. *Materials* **2019**, *12*, 726.
- (22) Tong, J.; Song, Z.; Kim, D. H.; Chen, X.; Chen, C.; Palmstrom, A. F.; Ndione, P. F.; Reese, M. O.; Dunfield, S. P.; Reid, O. G.; Liu, J.; Zhang, F.; Harvey, S. P.; Li, Z.; Christensen, S. T.; Teeter, G.; Zhao, D.; Al-Jassim, M. M.; van Hest, M. F. A. M.; Beard, M. C.; Shaheen, S. E.; Berry, J. J.; Yan, Y.; Zhu, K. Carrier Lifetimes of>1 μ s in Sn-Pb Perovskites Enable Efficient all-Perovskite Tandem Solar Cells. *Science* **2019**, *364*, 475–479.